

Automatic acute ischemic stroke lesion segmentation using semi-supervised learning

Bin Zhao^a, Hong Wu^a, Guohua Liu^a, Chen Cao^c, Song Jin^c, Zhiyang Liu^{a,*}, Shuxue Ding^{a,b,*}

^a Tianjin Key Laboratory of Optoelectronic Sensor and Sensing Network Technology, College of Electronic Information and Optical Engineering, Nankai University, Tianjin 300071, china

^b School of Artificial Intelligence, Guilin University of Electronic Technology, Guilin Guangxi 541004, china

^c Key Laboratory for Cerebral Artery and Neural Degeneration of Tianjin, Department of Medical Imaging, Tianjin Huanhu Hospital, Tianjin 300350, China

ABSTRACT

Ischemic stroke is a common disease in the elderly population, which can cause long-term disability and even death. However, the time window for treatment of ischemic stroke in its acute stage is very short. To fast localize and quantitatively evaluate the acute ischemic stroke (AIS) lesions, many deep-learning-based lesion segmentation methods have been proposed in the literature, where a deep convolutional neural network (CNN) was trained on hundreds of fully labeled subjects with accurate annotations of AIS lesions. Despite that high segmentation accuracy can be achieved, the accurate labels should be annotated by experienced clinicians, and it is therefore very time-consuming to obtain a large number of fully labeled subjects. In this paper, we propose a semi-supervised method to automatically segment AIS lesions in diffusion weighted images and apparent diffusion coefficient maps. By using a large number of weakly labeled subjects and a small number of fully labeled subjects, our proposed method is able to accurately detect and segment the AIS lesions. In particular, our proposed method consists of three parts: 1) a double-path classification net (DPC-Net) trained in a weakly-supervised way is used to detect the suspicious regions of AIS lesions; 2) a pixel-level K-Means clustering algorithm is used to identify the hyperintensive regions on the DWIs; and 3) a region-growing algorithm combines the outputs of the DPC-Net and the K-Means to obtain the final precise lesion segmentation. In our experiment, we use 460 weakly labeled subjects and 15 fully labeled subjects to train and fine-tune the proposed method. By evaluating on a clinical dataset with 150 fully labeled subjects, our proposed method achieves a mean dice coefficient of 0.639, and a lesion-wise F1 score of 0.799.

Keywords: semi-supervised learning, acute ischemic stroke lesion segmentation, convolutional neural network (CNN), K-Means, region growing

1. Introduction

Stroke has been one of the most common causes of death and long-term disability worldwide (Lopez et al., 2006), which brings tremendous pain and financial burden to patients. In general, stroke can be categorized as ischemia and hemorrhage according to the type of cerebrovascular accident, where ischemic stroke accounts for 87% of them (Benjamin et al., 2019). As the ischemic stroke may lead to invertible damage on brain tissues, in clinical practice, it is of paramount importance to quickly diagnose and quantitatively evaluate in the acute stage to improve the treatment outcome.

In diagnosing of ischemic strokes, magnetic resonance imaging (MRI) serves as the modality of choice for clinical evaluation. The diffusion weighted images (DWIs) and the apparent diffusion

* Corresponding author.

E-mail address: liuzhiyang@nankai.edu.cn (Z. Liu), sding@guet.edu.cn (S. Ding).

coefficient (ADC) maps derived from multiple DWI images with different b-values have been shown to be sensitive in diagnosing acute ischemic stroke (AIS). In particular, the AIS lesions appear as hyperintense on the DWIs and hypointense on the ADC maps (Yang et al., 2015). Fig. 1 presents some examples of AIS lesions. The regions identified by the red arrows are AIS lesions, while the regions identified by the yellow arrows are non-lesion regions, which are hyperintense on the DWIs as well. In fact, such hyperintensive regions are the magnetic susceptibility artifacts. That is to say, despite that they appear as hyperintense on the DWIs, there is no abnormality on the ADC maps, which indicates that such regions are artifacts, instead of AIS lesions. Therefore, to correctly identify the lesions, it is important to jointly consider both DWIs and ADC maps to extract the semantic information.

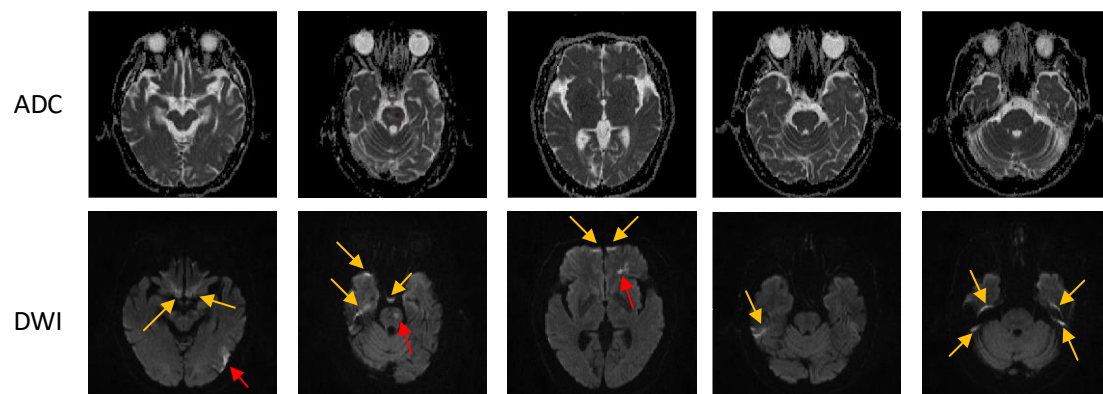


Figure 1. Challenge examples in AIS segmentation. The first row show ADC slices and the second row shows their corresponding DWI slices. The yellow arrows identify the hyperintense due to magnetic susceptibility artifacts, and the red arrows identify the hyperintense that are true AIS lesions. Best viewed in color.

Recently, convolutional neural network (CNN) based methods have presented tremendous ability in image classification and semantic segmentation on medical image processing (Dutil et al., 2015; Kamnitsas et al., 2015; Liu et al., 2019). Different from conventional image processing methods using handy-crafted image features, the CNN-based methods extract features from manually labeled data by itself. By training CNNs on a massive amount of labeled images, the CNN-based methods have achieved promising results on various organ and lesion segmentation tasks (Aslani et al., 2019; Roy et al., 2018; Sharma et al., 2017; Xu et al., 2018). In order to make use of contextual information in volumetric data, in (Hu et al., 2017), a 3D CNN was trained to automatically localize and delineate the abdominal organs of interest with a probability prediction map, and then a time-implicit multi-phase level-set algorithm was utilized for the refinement of the multi-organ segmentation. Another 3D CNN based method using fully convolutional DenseNet (Huang et al., 2017) was proposed for automatic segmentation of AIS (Zhang et al., 2018), which achieved high performance on their test set.

Typically in a CNN, millions of parameters have to be tuned, and therefore a massive amount of images with accurate annotations are required. For instance, (Sharma et al., 2017) used 165 fully labeled subjects to train its CNN for organ segmentation and (Zhang et al., 2018) collected 152 fully labeled subjects to train and validate its CNN for lesion segmentation. Different from the images in the ImageNet (Russakovsky et al., 2015) and COCO (Lin et al., 2014) dataset which can be easily obtained from the Internet and labeled by the ordinary people, the medical images have to be acquired by special equipment, and many well-trained clinicians are further required to precisely

annotate the labels. More importantly, to perform image segmentation, most methods require pixel-by-pixel annotations to train the CNN (Chen et al., 2014, 2017a; Hu et al., 2017; Ibtehaz and Rahman, 2019; Kamnitsas et al., 2015; Liu et al., 2018; Long et al., 2015; Milletari et al., 2016; Noh et al., 2015; Taha et al., 2018). For instance, in the AIS lesion segmentation tasks, most methods (Chen et al., 2017b; Liu et al., 2019; Zhang et al., 2018) required subjects with pixel-wise labels as shown in Fig. 2, where each pixel was classified as normal or lesion. Obviously, annotating the pixel-labels are labor-intensive and time-consuming, making it even difficult to establish a large dataset. This motivates us to develop a segmentation method by using much simpler annotations. One of the simpler annotations is just annotating whether each slice incorporates lesions or not, as shown in Fig. 3. Hereafter, we term this simpler annotation as weak annotation, and the data obtained is termed as weakly labeled. Since the clinicians only require annotating whether each slice includes AIS lesions or not, which significantly reduce the cost on annotation, and making it more possible to collect a large amount of labeled data samples.

What is very challenging is whether such data really can be used to train a well performed CNN. For answer this, in this paper, a semi-supervised segmentation method is proposed. As depicted in Fig. 4, our proposed method includes three components: the DPC-Net, K-Means algorithm and region-growing algorithm. In particular, the DPC-Net is a CNN that identify the suspicious AIS lesion regions and outputs a probability map (PM) for each image slice, by using the semantic information extracted from the weakly labeled images. Parallely, the corresponding DWIs are input to the K-Means algorithm for generating pixel-level segmentation by using the fact that the AIS lesions appear as hyperintense on the DWIs. Finally, the region-growing algorithm combines the results of DPC-Net and the K-means clustering to precisely segment the AIS lesions. A small number of fully labeled images are used to tune the hyperparameters for K-means clustering and the region-growing algorithms to refine the segmentation results. In this paper, we collected 460 weakly labeled subjects and 15 fully labeled subjects to train and to fine-tune the algorithm.

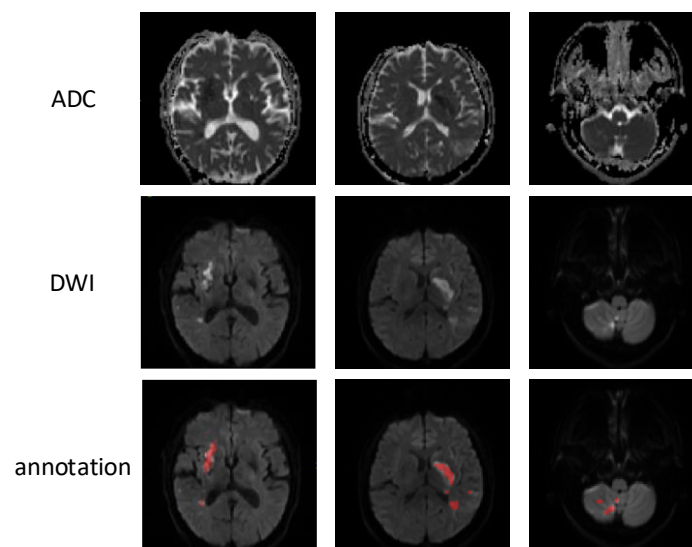


Figure 2. Examples of the fully labeled subjects. The first two rows show ADC slices and their corresponding DWI slices. The third row shows the annotations. Best viewed in color.

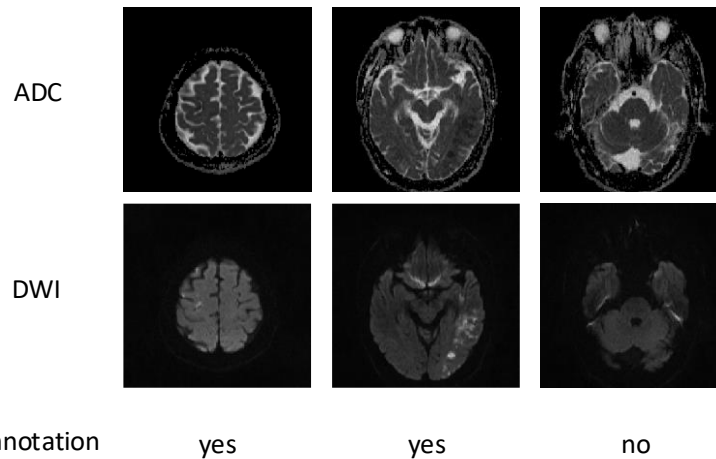


Figure 3. Examples of the weakly labeled subjects. The first two rows show ADC slices and their corresponding DWI slices. The third row shows the annotations, “yes” indicates that the slice has lesion and “no” indicates the opposite.

2. Related work

There have been efforts on automatic segmentation of ischemic stroke lesion recently. We roughly divided these methods into two categories, conventional methods and CNN based methods, according to whether handy-crafted features are required. In the conventional methods, by defining some specific features on the MRIs, the ischemic stroke lesions can be identified by conventional image processing techniques or using machine-learning algorithms such as the random forest or the support vector machine (SVM). For instance, a gravitational histogram optimization based method was proposed for ischemic stroke lesion segmentation using DWI (Nabizadeh et al., 2013). To reduce the false positive rate, (Mitra et al., 2014) further proposed to use multimodal MRIs to extract features and identify the lesions using random forest. In (Maier et al., 2014), a stroke lesion segmentation method based on local features extracted from multimodal MRI, and a support vector machine (SVM) classifier was further trained to segment the lesions. The random-forest-based method was further used to identify the sub-acute ischemic stroke lesions (Mahmood and Basit, 2015), which was among the top-ranking methods in Ischemic Stroke Lesion Segmentation (ISLES) challenge in 2015 (Maier et al., 2017). Although those methods have been very successful, it appears that their modelling capabilities are still significantly limited. For instance, handy-crafted features are required. Therefore the performances of the methods are still not good enough, which is understandable by the results of the recent challenge in ISLES 2015 (Maier et al., 2017).

At the same time, CNN based methods have emerged as a powerful alternative for automatic segmentation of ischemic stroke lesion. The challenge of sub-acute ischemic stroke lesion segmentation in ISLES 2015 attracted many entries and most of the entries are CNN based methods. Among the top ranked approaches, DeepMedic (Kamnitsas et al., 2017) based on a multi-scale 3D CNN with fully contested CRFs achieved a dice coefficient of 0.59 on testing set, which won the ISLES 2015 challenge. Some other successful methods (Liu et al., 2018; Zhang et al., 2018) based on CNNs in ISLES 2015 also derived from generic CNNs architecture. Nevertheless, sub-acute ischemic stroke lesions have different imaging modality and lesion features from AIS lesions, so that the methods can not be straightforwardly generalized to be used for AIS lesions. It is necessary to explore the methods for segmentation of AIS lesion.

Due to the lack of public dataset on the AIS lesion segmentation task, the evaluation results on the institutional data were reported in the literature only. A framework (Chen et al., 2017b) with the

combination of EDD Net and multiscale convolutional label evaluation net (MUSCLE Net) achieved a dice coefficient of 0.67 on testing set using DWI. In order to make further use of MRI information, Res-CNN (Liu et al., 2019) carried out segmenting AIS lesion in multi-modality MRI. To take advantage of contextual information in volumetric data, a method based on 3D fully CNNs was proposed for AIS lesion segmentation (Zhang et al., 2018), which achieved a high performance. However, this method requires a large amount of high quality fully labeled subjects, which are difficult to obtain.

Interestingly, some weakly-supervised methods have attracted extensive attention in cancer histopathology image segmentations (Jia et al., 2017; Xu et al., 2014), where the clinicians only need to annotate whether an image contains cancer cells or not. In the weakly supervised learning, however, since the CNN was originally trained as a classifier, it is probable to only identify the most prominent feature that helps in classification, which makes it possible to underestimate the lesion size when the lesion is large. On the other hand, in the weakly supervised learning, the final segmentation results are obtained from the output of the last convolution layer to make use of the semantic information. As the resolution of output feature map in the last convolution layer is much lower than the input image, the sizes of the small lesions are typically overestimated. Therefore, when applying to the AIS lesion segmentation, as the lesion size varies in a large range, the segmentation results would be quite inaccurate for quantitatively evaluating the lesion size. To improve the accuracy, in this paper, we propose to use a semi-supervised learning method by using a small number of fully labeled images to fine-tune the segmentation results. In this paper, we use 460 weakly labeled subjects and 30 fully labeled subjects to train and fine-tune our proposed method, which achieves competitive results on the testing set.

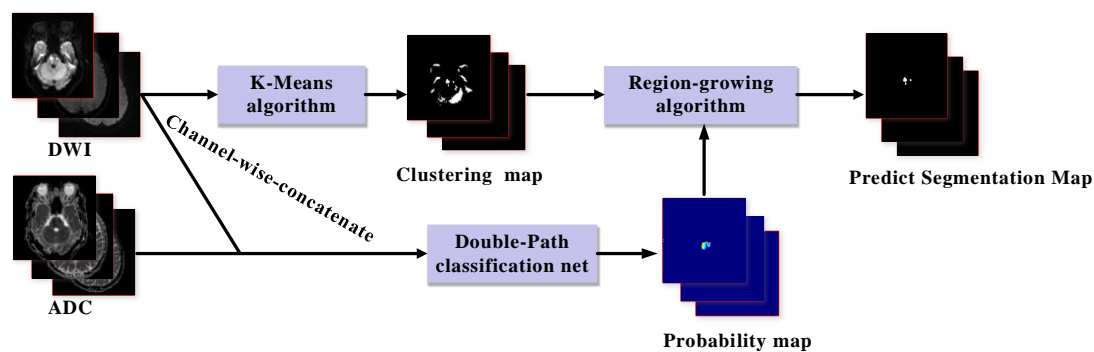


Figure.4 Architecture of the proposed semi-supervised for lesion segmentation. The red box is added to distinguish each image. The color map of probability map is “jet”. Best viewed in color.

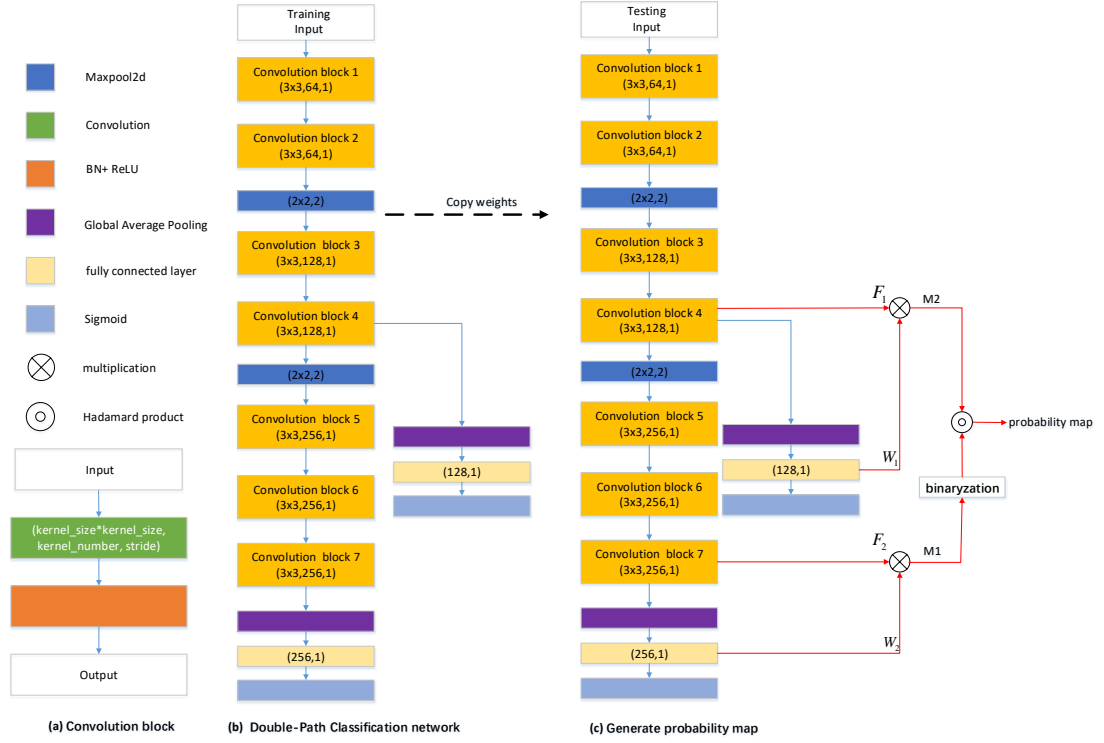


Figure 5. Our proposed method for generating probability maps. Best viewed in color.

3. Methods

In this section, we present a semi-supervised deep learning method for AIS lesion segmentation on multi-modal MR images, and the whole pipeline is presented in Fig. 4. In particular, our proposed method includes two pathways. In the first pathway, we propose a double-path classification network (DPC-Net) to extract semantic information from the weakly labeled subjects. Remarkably, despite that the network is trained on the slice-wise label as a classifier, during the inference stage, this network architecture is able to not only identify problematic slices, but also roughly detect the regions with AIS lesions. In the other pathway, a K-Means clustering algorithm is incorporated to obtain the lesion segmentation results. Then, a region-growing algorithm is adopted to combine the results of the two pathways and generate the final segmentation result. Intuitively, a deep CNN is able to extract semantic information of AIS lesions at the expense of the spatial information loss, while a naive image clustering algorithm preserves as much as possible spatial context, however, with little semantic information. As we will show in this paper, the segmentation results can be significantly improved by properly incorporating the results from the two pathways.

3.1 Double-Path Classification Network

The DPC-Net is proposed based on the VGG-16 network (Simonyan and Zisserman, 2014) truncated before the third maxpooling layer, and the network architecture is depicted in Fig. 5b. As we can see, we added a global average pooling (GAP) layer followed by a fully connected (FC) layer at the top of the network. Intuitively, the feature maps of the convolution block 7 is much lower than the original input images, leading to an inaccurate output probability map from the view of segmentation task. To this end, we further added a side-branch with a GAP layer and a FC layer on convolution block 4 to improve the spatial resolution. As we will see in Section 4, despite that the side-branch output may contain many false positives due to the lack of semantic information, the segmentation results can be significantly improved by combining the outputs of the main-branch

and the side-branch.

At the training stage, as only the slice-level label is available, a classifier is trained by using the DPC-Net shown in Fig. 5b, which can be regarded as a weakly-supervised learning in the viewpoint of the AIS lesion segmentation. At the predicting stage, as our objective is to locate the AIS lesions, the class activation maps (CAMs) (Zhou et al., 2016) is computed for both the main and the side branches to generate the segmentation seeds with adequate semantic information to highlight suspicious lesion region.

In particular, as Fig. 5c shows, the weighted sums of the output feature maps of both conv-block 7 and conv-block 4 are computed to generate two CAMs, denoted as M_1 and M_2 , respectively, where the weights are copied from the corresponding FC layers. To ensure that the maximum activations equals one, the CAMs are further normalized as

$$\bar{M}_i = \begin{cases} M_i / \max M_i & , \hat{y} \geq 0.5 \\ 0, & \hat{y} < 0.5 \end{cases}$$

for $i = 1, 2$, where \hat{y} denotes the main branch output of the classifier.

Note that the main branch CAM output M_1 has a low spatial resolution with, however, more semantic information. We propose to fuse both CAMs to achieve a more accurate segmentation of the lesion regions. We first compute a binary segmentation map M_{1b} from the main branch CAM output M_{1b} by a threshold of 0.5, and then fuse M_{1b} and M_2 to generate PM as

$$PM = M_{1b} \circ M_2,$$

where \circ denotes the Hadamard product.

3.2 Pixel level clustering

The K-Means is an unsupervised machine-learning algorithm that partition a set of vectors into K groups that cluster around a common mean vector. When applying to a single image, it can be interpreted as a segmentation method that clusters image pixels with similar intensities to the same groups, making it accurate in segmenting the lesions with distinguished intensity property. On the other hand, different from the deep-learning-based segmentation, the K-Means clustering focus only on the pixel intensities, and no semantic information is considered, leading to many false positives in lesion segmentation.

In this paper, by making use of the expert knowledge in AIS lesion detection that the AIS lesions appear as hyperintense on the DWIs (Yang et al., 2015), we propose to adopt K-Means algorithm and a region-growing algorithm to identify the lesion regions. Our proposed algorithm is summarized as follows:

1. Initialize a segmentation result $\mathbf{Q} = \mathbf{0}$.
2. K-Means algorithm is adopted on the DWI to cluster the pixels into K groups. By preserving the group with the largest pixel values, a clustered image \mathbf{I} is obtained.
3. Perform connected component analysis on \mathbf{I} , and identify all connected regions, denoted as L_i , for $i = 1, 2, \dots$
4. Select a point \mathbf{x} with $PM(\mathbf{x}) \geq \delta$.
5. If $\mathbf{x} \notin L_i, \forall i$, return to step 4. If $\mathbf{x} \in L_k$, set $\mathbf{Q}(\mathbf{y}) = 1, \forall \mathbf{y} \in L_k$.
6. Repeat step 4-5, until all points on PM are examined.

The proposed algorithm integrates both the pixel-level information of the original DWIs and the

semantic information extracted by the DPC-Net. To achieve a better performance, the key problem is how to determine the number of clusters K and the threshold δ . In this paper, we propose to use some fully labeled subjects to fine-tune these two parameters by using grid search method. As we will discussed in the next section, the segmentation results can be significantly improved by using a very small amount of fully labeled images.

3.3 Evaluation Metrics

In this paper, we propose to use dice coefficient (DC) to evaluate the segmentation performance, which is defined as

$$DC = \frac{2|G \cap P|}{|G| + |P|},$$

where G and P denote the ground truth and the predicted segmentation, respectively. $|\cdot|$ denotes the region of lesion segmentation.

In clinical diagnosis, the segmentation results on both large and small lesions are of equal importance. It is therefore necessary to use the lesion-wise metrics to evaluate the performance. In particular, we perform 3D connected component analysis on both the ground truth and the predicted segmentation. A region is said to be a true positive (TP) if it appears on both ground truth and the prediction. A false positive (FP) is counted if a region on the prediction has no overlapping area with any region on the ground truth; while a false negative (FN) is counted if a region appears on the ground truth has no overlapping area with any region on the prediction. The mean number of TPs (m#TP), the mean number of FPs (m#FP) and the mean number of FNs (m#FN) can be then calculated by averaging over the total number of subjects.

In addition, we further propose the lesion-wise precision rate (P_L), the lesion-wise recall rate (R_L) and the lesion-wise F1 score as metrics, which are given as

$$P_L = \frac{m\#TP}{m\#TP + m\#FP},$$

$$R_L = \frac{m\#TP}{m\#TP + m\#FN},$$

and

$$F1 = \frac{2P_L \cdot R_L}{P_L + R_L},$$

respectively.

4. Experiment and Results

4.1 Data and pre-processing

The experimental data used in this study is from Nankai University affiliated Tianjin Huanhu Hospital, which includes 640 patients with AIS lesions. All clinical images were collected from a retrospective database and anonymized prior to use. Ethical approval was granted by Tianjin Huanhu Hospital Medical Ethics Committee. MR images were acquired from three MR scanners, with two 3T MR scanners (Skyra, Siemens and Trio, Simens) and one 1.5T MR scanner (Avanto, Siemens). DWI images were acquired using a spin-echo type echo-planar (SE-EPI) sequence with b values of 0 and 1000 s/mm². The parameters are summarized in Tab.1. ADC maps were calculated from the scan raw data in a pixel-by-pixel manner as

$$ADC = \frac{\ln S_1 - \ln S_0}{b_1 - b_0}$$

where b is the diffusion-sensitizing gradient pulses, with $b_1 = 1000$ s/mm² and $b_0 = 0$ s/mm² in our data. S_1 is the diffusion-weighted signal intensity with $b = 1000$ s/mm². S_0 is the signal with no diffusion gradient applied, I.e., with $b = 0$ s/mm².

Table 1. Parameters used in DWI acquisition.

MR scanners	Skyra	Trio	Avanto
Repetition time (ms)	5200	3100	3800
Echo time (ms)	80	99	102
Flip angle (°)	150	120	150
Number of excitations	1	1	3
Field of view (mm ²)	240 × 240	200 × 200	240 × 240
Matrix size	130 × 130	132 × 132	192 × 192
Slice thickness (mm)	5	6	5
Slice spacing (mm)	1.5	1.8	1.5
Number of slices	21	17	21

The DWI and ADC images were copy referenced to ensure the same slice position so as to allow optimal image evaluation and measurement. The ischemic lesions were manually labeled by two experienced experts (Dr. Song Jin and Dr. Chen Cao) from Nankai University Affiliated Tianjin Huanhu Hospital. We split the whole dataset into two subsets: training set and test set. The training set includes 460 subjects with slice-level labels for training and validating the DPC-Net, and 30 subjects with pixel-level labels to fine-tune clustering number K in the K-Means algorithm and the threshold value δ in the region growing algorithm. The test set includes 150 subjects with pixel-level labels to evaluate the segmentation performance.

As the MR images were acquired on the three different MR scanners, the matrix size varies. Therefore, we resample all the MR images to the same size of 192 × 192 using linear interpolation. The pixel intensity of each MR image slice is normalized into that of zero mean and unit variance, and the DWI and ADC slices are concatenated into a 2-channel images and fed into the DPC-Net. During training, data augmentation technique is adopted to avoid over-fitting. In particular, each input image is randomly rotated by a degree ranging from 1 to 360 degree, flipped vertically and horizontally on the fly, so as to augment the dataset and reduce memory footprint.

4.2 Setup and Implementation

The hyperparameters of the proposed DPC-Net are shown in Fig.5. We initialize these networks by Xavier method (Glorot and Bengio, 2010) and use the Adam method (Kingma and Ba, 2014) with initial learning rate of 0.001, $\beta_1 = 0.9$, $\beta_2 = 0.999$ as our optimizer. The learning rate is scaled down by a factor of 0.1 if no progress is made for 15 epochs on validation loss. Early-stopping technique is adopted after 30 epochs with no progress on the validation loss.

The experiments are performed on a computer with an Intel Core i7-6800K CPU, 64GB RAM and Nvidia GeForce 1080Ti GPU with 11GB memory. The computer operates on Windows 10 with CUDA 9.0. The network is implemented on PyTorch 0.4¹ and K-Means is implemented on scikit-learn². The MR image files are stored as Neuroimaging Informatics Technology Initiative (NIfTI)

¹ <https://pytorch.org/>

² <https://scikit-learn.org/stable/>

format, and processed using Simple Insight ToolKit (SimpleITK) (Lowekamp et al., 2013). We use ITK-SNAP (Yushkevich et al., 2006) for the visualization of results.

4.3 Results

In our experiment, 460 weakly labeled subjects and 30 fully labeled subjects are used to train and fine-tune the parameters. The 30 fully labeled subjects are abbreviated as fine-tuning set. Fig. 6 presents the segmentation results of our proposed method. The CAM results obtained from a naïve CAM method (Zhou et al., 2016), the output CAM of VGG-16 net denoted as CAM-baseline, and the fused CAM output PM of our proposed DPC-Net, denoted as PM-DPC, are also presented for comparison. As shown in Fig. 6, the CAM-based methods can successfully identify and localize the AIS lesions. Despite that the magnetic artifacts have similar appearances as the AIS lesions on the DWIs, the deep-learning-based methods can distinguish the lesions from the artifacts thanks to the semantic information extracted from the weakly-labeled subjects. From the aspect of segmentation, however, the conventional CAM method, denoted as CAM-baseline in Fig. 6, tends to segment much larger area than the actual AIS lesion, due to the fact that the output feature maps in conventional CAM method is much lower than the original images. Our proposed DPC-Net significantly reduces the areas of the suspicious regions thanks to the side branch output, but underestimates the lesion areas in some cases. By integrating both pixel-level clustering and the PM-DPC output, the proposed method is sensitive to both large and small lesions, and presents much better segmentation results over the CAM-baseline and PM-DPC.

The numerical evaluation results on the testing set with 150 fully labeled subjects are summarized in Tab. 2. For CAM-baseline and PM-DPC, the thresholds to generate the binary segmentation are selected by using the fine-tuning set. For our proposed method, these fully labeled images are used to tune both the threshold δ and the number of clusters K . As Table 2 shows, our proposed method achieves the best results on testing set. From the aspect of the pixel-level metrics, our proposed method achieves a DC of 0.639, which is much higher than the results obtained by CAM-baseline and PM-DPC. In fact, such performance is very close to the method trained on fully labeled images (Chen et al., 2017b). From the aspect of lesion-wise metrics, our proposed method achieves the highest precision rate over the CAM-baseline and the PM-DPC. The recall rate, however, is slightly worse than the CAM-baseline due to the fact that the CAM-baseline tends to annotate a very large area. The K-Means clustering algorithm may also fail to group all lesions to the same group if the intensities of different lesions differ significantly from each other.

Table 2. The evaluation measurements on testing set.³

methods	CAM-baseline	PM-DPC	Our semi-supervised method
(δ, K)	(0.7,-)	(0.3,-)	(0.41,6)
DC	0.091	0.475	0.639
P_L	0.854	0.790	0.870
R_L	0.791	0.742	0.738
$F1$	0.821	0.765	0.799

³ - indicates that the method does not have this parameter K .

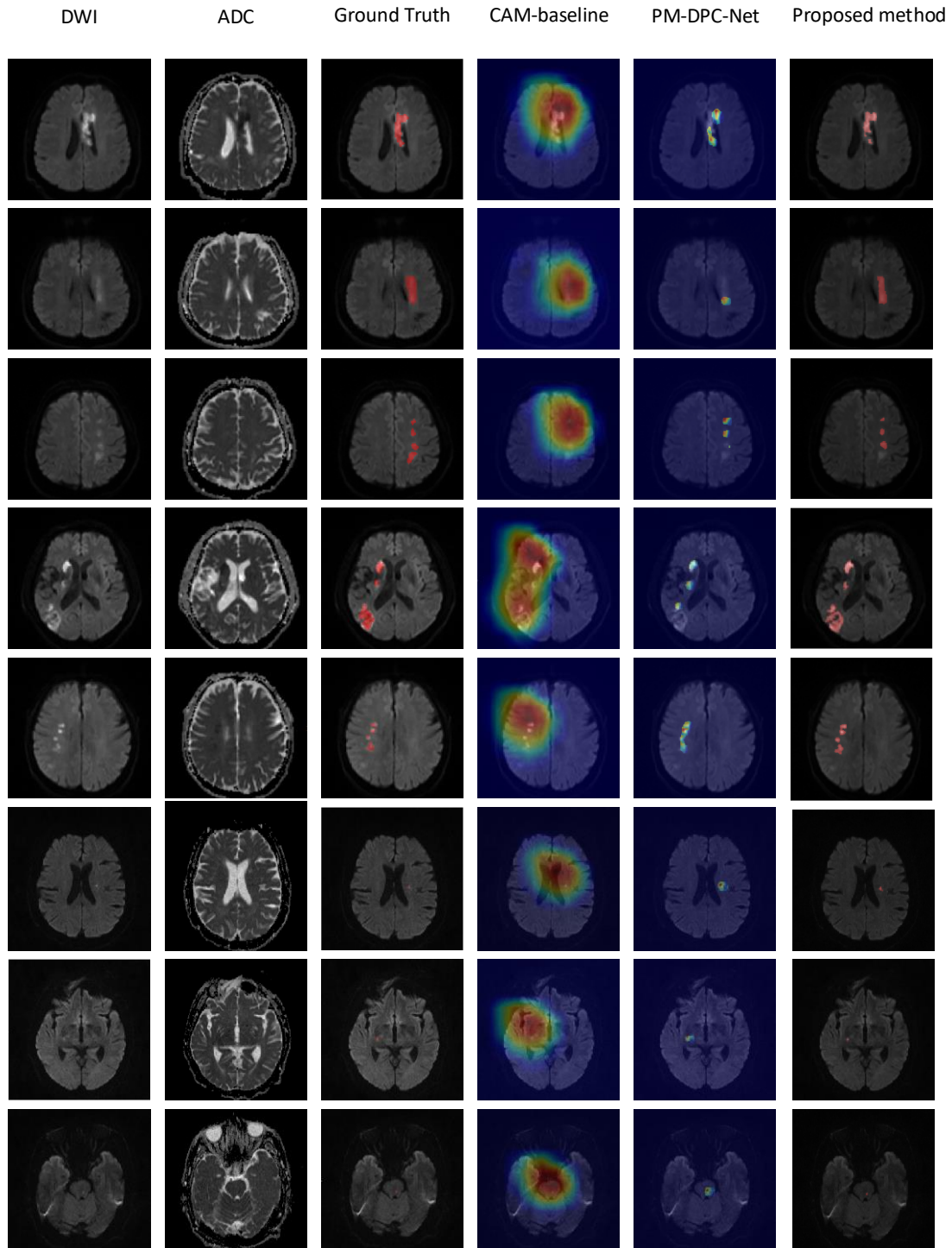


Figure 6. Examples of lesion segmentation, CAMs and PMs. The first two columns show the original DWI and ADC images, respectively. The third and the sixth columns show the manually labeled lesions and the segmentation results of our semi-supervised method, respectively. The fourth column shows the CAMs of the baseline VGG-16 Network (CAM-baseline (Zhou et al., 2016)), and the fifth column shows the PMs of DPC Network (PM-DPC-Net). The CAMs and PMs are depicted on the DWI, and the redder with the color map, the more likely it is to represent the lesion region. The segmentations are also depicted on the DWI, and highlighted in red. Best view in color.

5. Discussions

5.1 Effect of the number of K-Means clusters K

As the AIS lesions appear as hyperintense on the DWI, we adopt K-Means clustering algorithm to identify the hyperintensive regions. Note that the artifacts on the DWIs are also the hyperintensive regions, making it crucial to fine tune the value of K . As we can see from Fig. 7, when $K = 4$, more artifacts will be in the same cluster as the AIS lesions including the artifacts around the lesions, thus, the clustering lesion regions will be larger than the true lesions. As the K increases, the clustering lesion regions will gradually decrease from greater than the true lesion regions to the near true lesion regions, and then to less than the true lesion regions until some clustering lesion regions disappear. The first row and the fourth row in Fig. 7 show that some clustering lesion regions have disappeared when $K = 7$.

In our work, we propose to use a small amount of fully labeled subjects to search the optimal parameters in a grid search manner, and use DC as the metric. The results with $K = 4, 5, 6$ and 7 are summarized in Table 3. As we can see from Table 3, the threshold δ increases with the increase of K when $K = 4, 5, 6$, meanwhile, the evaluation results also increase. However, the threshold δ reduces to 0.25 when $K = 7$. This phenomenon indicates that when the clustering lesion regions reduce to the near true lesion regions, the predicted suspicious lesion regions in corresponding M_{fuse} should have small intersections with the clustering lesion regions in clustering maps. However, when some clustering lesion regions disappear, the predicted suspicious lesion regions in corresponding PM will expand its lesion regions. The optimal clustering number leads to the best clustering results in general.

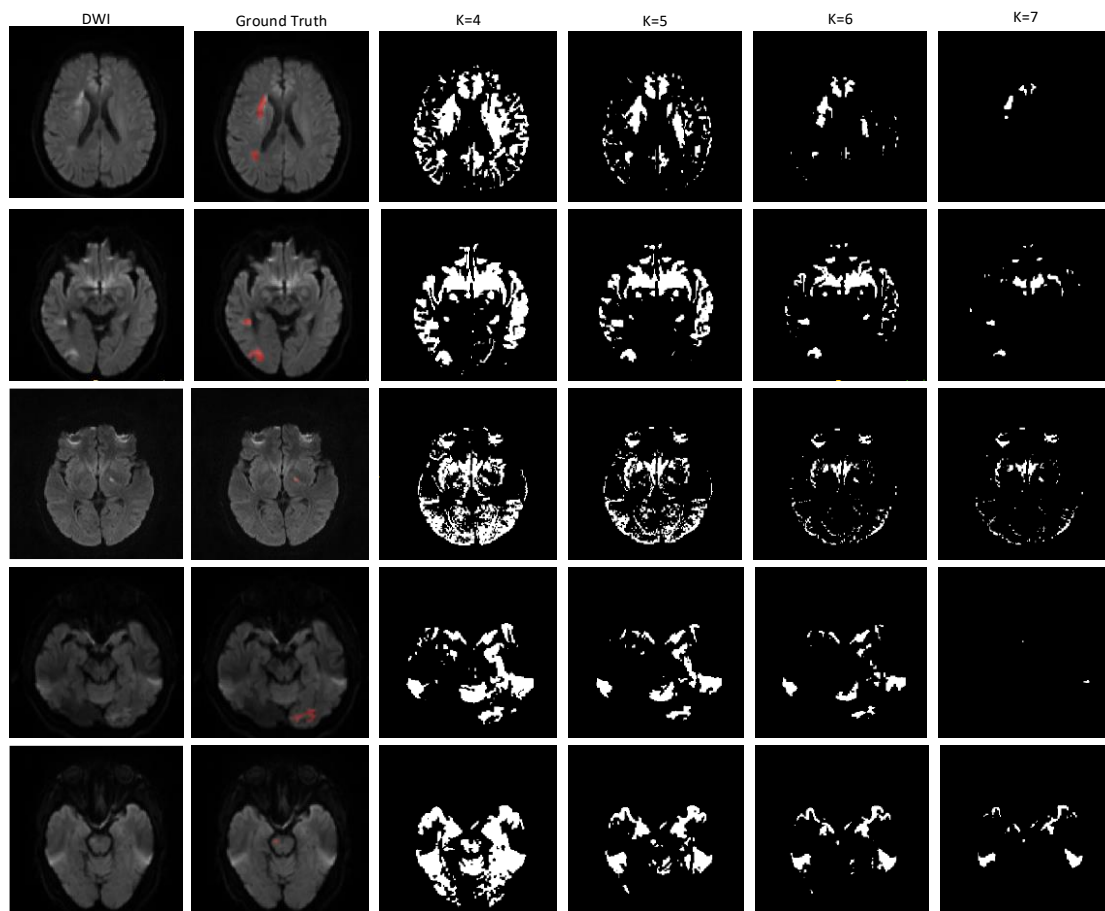


Figure 7. Examples of clustering map. The first two columns show the original DWI and the manually labeled lesions, respectively. The last four columns show the clustering maps with the clustering number of 4,5,6 and 7, respectively.

Table 3. Evaluation results under the variety of K and δ on fine-tuning set and on testing set.

(δ, K)	(0.23,4)		(0.29,5)		(0.41,6)		(0.25,7)	
Data set	Fine-tuning set	Testing set	Fine-tuning set	Testing set	Fine-tuning set	Testing set	Fine-tuning set	Testing set
DC	0.375	0.319	0.548	0.593	0.575	0.639	0.504	0.610
P_L	0.857	0.804	0.879	0.806	0.906	0.870	0.865	0.866
R_L	0.761	0.846	0.718	0.782	0.676	0.738	0.634	0.698
$F1$	0.806	0.825	0.791	0.794	0.774	0.799	0.732	0.773

5.2 How many fully labeled subjects do we need?

In Section 4, we use 30 fully labeled subjects to fine-tune the clustering number on DWI and threshold for fused CAM PM. In this subsection, we will investigate whether we can further reduce the number of fully labeled subjects. In particular, we randomly select 10, 15 and 20 fully labeled subjects out from the 30 fully labeled subjects to search for the optimal K and threshold δ . Table 4 summarizes the search results. As we can see from Tab. 4, we can achieve the same optimal parameters even when only 15 subjects is used. When the number of subjects is 10, the optimal parameters are 5 and 0.29, the corresponding evaluation measurements of testing set are $DC = 0.593, P_L = 0.806, R_L = 0.782$ and $F1 = 0.794$, which are the competitive results with the best results in Table 4.

Table 4. The optimal parameters and the evaluation results on the 20, 15, and 10 subjects, respectively.

(δ, K)	(0.41,6)		(0.41,6)		(0.29,5)	
Data set	20 subjects	Testing set	15 subjects	Testing set	10 subjects	Testing set
DC	0.564	0.639	0.558	0.639	0.544	0.593
P_L	0.949	0.870	0.935	0.870	0.870	0.806
R_L	0.617	0.738	0.569	0.738	0.614	0.782
$F1$	0.747	0.799	0.707	0.799	0.720	0.794

5.3 Performance on large and small lesions on experimental results

According to the article (Lodder, 2007), a AIS lesion is classified as a lacunar infarction (LI) lesion if its diameter is smaller than 1.5cm. Clinically, the LI stroke accounts for 85% of all AIS patients. However, it is much difficult to be diagnosed in clinical practice, especially when it is too small to be noticed. It is, therefore, very necessary to evaluate the performance on small lesions.

In our test set, there are 60 subjects with large lesions and 90 subjects with small lesions. As Tab. 5 shows, our proposed method achieves a DC of 0.706 on the 60 subjects with small lesions, while a DC of 0.538 on the 90 subjects with large lesions. Meanwhile, the R_L of small lesions is higher than that of large lesions, the reason for that is the distribution of hyperintense in large lesion regions are uneven, which leads the lesion regions predicted by DPC-Net to be smaller than the true lesion regions. Moreover, clustering maps on DWI focus on hyperintense only. Thus, how to solve the influence of hyperintense distribution imbalance on lesion segmentation is a problem to be considered in the future.

In clinical diagnosis, large lesions are more easily diagnosed, while small lesions are not. Our proposed method achieves high performance on small lesions, which might be of a good inspiration for other methods.

Table 5. Evaluation results on testing set, large lesions set and small lesions set, respectively.

Data set	Testing set	Large lesions set	Small lesions set
DC	0.639	0.538	0.706
P_L	0.870	0.871	0.867
R_L	0.738	0.656	0.929
$F1$	0.799	0.749	0.897

6. Conclusion

In this paper, we present a semi-supervised method for AIS lesion segmentation, where 460 weakly labeled subjects are used to train the DPC-Net and then 15 fully labeled subjects are used to fine-tune the parameters in a supervised way. The DWI and ADC are used as input of our proposed DPC-Net and the DWI from are used as input of K-Means to generate clustering maps.

The proposed semi-supervised method presents a high segmentation accuracy on the clinical MR images with a dice coefficient of 0.639. More importantly, it presents very high precision of 0.870, which is of paramount importance in avoiding misdiagnosis in clinical scenario. Meanwhile, the proposed method largely reduces the expense of obtaining a large number of fully labeled subjects in a supervised setting, which is more meaningful in terms of engineering maneuverability.

6. Acknowledgement

This work is supported in part by the National Natural Science Foundation of China [grant numbers 61871239, 61571244 and 61671254], and in part by the Fundamental Research Funds for the Central Universities, Nankai University [grant number 63191106].

References

- Aslani, S., et al., 2019. Multi-branch convolutional neural network for multiple sclerosis lesion segmentation. *Neuroimage* 196, 1-15.
- Benjamin, E.J., et al., 2019. Heart Disease and Stroke Statistics-2019 Update: A Report From the American Heart Association. *Circulation* 139, e56-e528.
- Chen, L.-C., Papandreou, G., Kokkinos, I., Murphy, K., Yuille, A.L., 2014. Semantic image segmentation with deep convolutional nets and fully connected crfs. *arXiv preprint arXiv:1412.7062*.
- Chen, L.-C., Papandreou, G., Kokkinos, I., Murphy, K., Yuille, A.L., 2017a. Deeplab: Semantic image segmentation with deep convolutional nets, atrous convolution, and fully connected crfs. *IEEE Transactions on Pattern Analysis and Machine Intelligence* 40, 834-848.
- Chen, L., Bentley, P., Rueckert, D., 2017b. Fully automatic acute ischemic lesion segmentation in DWI using convolutional neural networks. *NeuroImage: Clinical* 15, 633-643.
- Dutil, F., Havaei, M., Pal, C., Larochelle, H., Jodoin, P., 2015. A convolutional neural network approach to brain lesion segmentation. *Ischemic Stroke Lesion Segmentation*, 51-56.
- Glorot, X., Bengio, Y., 2010. Understanding the difficulty of training deep feedforward neural networks. *Proceedings of the thirteenth international conference on artificial intelligence and statistics*, pp. 249-256.
- Hu, P., et al., 2017. Automatic abdominal multi-organ segmentation using deep convolutional neural network and time-implicit level sets. *International Journal of Computer Assisted Radiology and Surgery* 12, 399-411.

Huang, G., Liu, Z., Weinberger, K.Q., 2017. Densely Connected Convolutional Networks. 2017 IEEE Conference on Computer Vision and Pattern Recognition (CVPR), 2261-2269.

Ibtehaz, N., Rahman, M.S., 2019. MultiResUNet: Rethinking the U-Net Architecture for Multimodal Biomedical Image Segmentation. arXiv preprint arXiv:1902.04049.

Jia, Z., Huang, X., Chang, E.I., Xu, Y., 2017. Constrained Deep Weak Supervision for Histopathology Image Segmentation. IEEE Transactions on Medical Imaging 36, 2376-2388.

Kamnitsas, K., Chen, L., Ledig, C., Rueckert, D., Glocker, B., 2015. Multi-scale 3D convolutional neural networks for lesion segmentation in brain MRI. Ischemic Stroke Lesion Segmentation 13, 46.

Kamnitsas, K., et al., 2017. Efficient multi-scale 3D CNN with fully connected CRF for accurate brain lesion segmentation. Medical Image Analysis 36, 61-78.

Kingma, D.P., Ba, J., 2014. Adam: A method for stochastic optimization. arXiv preprint arXiv:1412.6980.

Lin, T.-Y., et al., 2014. Microsoft coco: Common objects in context. European conference on computer vision. Springer, pp. 740-755.

Liu, L., et al., 2019. Deep convolutional neural network for automatically segmenting acute ischemic stroke lesion in multi-modality MRI. Neural Computing and Applications.

Liu, Z., et al., 2018. Towards Clinical Diagnosis: Automated Stroke Lesion Segmentation on Multi-Spectral MR Image Using Convolutional Neural Network. IEEE Access 6, 57006-57016.

Lodder, J., 2007. Size criterion for lacunar infarction. Cerebrovascular Diseases 24, 156.

Long, J., Shelhamer, E., Darrell, T., 2015. Fully convolutional networks for semantic segmentation. Proceedings of the IEEE conference on computer vision and pattern recognition, pp. 3431-3440.

Lopez, A.D., Mathers, C.D., Ezzati, M., Jamison, D.T., Murray, C.J., 2006. Global and regional burden of disease and risk factors, 2001: systematic analysis of population health data. Lancet 367, 1747-1757.

Lowekamp, B., Chen, D., Ibanez, L., Blezek, D., 2013. The design of simpleITK.

Mahmood, Q., Basit, A., 2015. Automatic ischemic stroke lesion segmentation in multi-spectral MRI images using random forests classifier. BrainLes 2015. Springer, pp. 266-274.

Maier, O., et al., 2017. ISLES 2015-A public evaluation benchmark for ischemic stroke lesion segmentation from multispectral MRI. Medical Image Analysis 35, 250-269.

Maier, O., Wilms, M., von der Gablentz, J., Krämer, U., Handels, H., 2014. Ischemic stroke lesion segmentation in multi-spectral MR images with support vector machine classifiers. Medical Imaging 2014: Computer-Aided Diagnosis. International Society for Optics and Photonics, p. 903504.

Milletari, F., Navab, N., Ahmadi, S.-A., 2016. V-net: Fully convolutional neural networks for volumetric medical image segmentation. 2016 Fourth International Conference on 3D Vision (3DV). IEEE, pp. 565-571.

Mitra, J., et al., 2014. Lesion segmentation from multimodal MRI using random forest following ischemic stroke. Neuroimage 98, 324-335.

Nabizadeh, N., Kubat, M., John, N., Wright, C., 2013. Automatic ischemic stroke lesion segmentation using single mr modality and gravitational histogram optimization based brain segmentation. Proceedings of the International Conference on Image Processing, Computer Vision, and Pattern Recognition (IPCV). The Steering Committee of The World Congress in Computer Science, Computer ..., p. 1.

Noh, H., Hong, S., Han, B., 2015. Learning deconvolution network for semantic segmentation. Proceedings of the IEEE international conference on computer vision, pp. 1520-1528.

Roy, S., Butman, J.A., Reich, D.S., Calabresi, P.A., Pham, D.L., 2018. Multiple sclerosis lesion segmentation from brain MRI via fully convolutional neural networks. arXiv preprint arXiv:1803.09172.

Russakovsky, O., et al., 2015. Imagenet large scale visual recognition challenge. International Journal of Computer Vision 115, 211-252.

Sharma, K., et al., 2017. Automatic Segmentation of Kidneys using Deep Learning for Total Kidney Volume Quantification in Autosomal Dominant Polycystic Kidney Disease. Scientific Reports 7, 2049.

Simonyan, K., Zisserman, A., 2014. Very Deep Convolutional Networks for Large-Scale Image Recognition. Computer Science.

Taha, A., Lo, P., Li, J., Zhao, T., 2018. Kid-Net: convolution networks for kidney vessels segmentation from CT-volumes. International Conference on Medical Image Computing and Computer-Assisted Intervention. Springer, pp. 463-471.

Xu, B., et al., 2018. Orchestral fully convolutional networks for small lesion segmentation in brain MRI. 2018 IEEE 15th International Symposium on Biomedical Imaging (ISBI 2018). IEEE, pp. 889-892.

Xu, Y., et al., 2014. Weakly supervised histopathology cancer image segmentation and classification. Medical Image Analysis 18, 591-604.

Yang, J., et al., 2015. Risk factors for incident dementia after stroke and transient ischemic attack. Alzheimers Dement 11, 16-23.

Yushkevich, P.A., et al., 2006. User-guided 3D active contour segmentation of anatomical structures: significantly improved efficiency and reliability. Neuroimage 31, 1116-1128.

Zhang, R., et al., 2018. Automatic segmentation of acute ischemic stroke from DWI using 3-D fully convolutional DenseNets. IEEE Transactions on Medical Imaging 37, 2149-2160.

Zhou, B., Khosla, A., Lapedriza, A., Oliva, A., Torralba, A., 2016. Learning deep features for discriminative localization. Proceedings of the IEEE conference on computer vision and pattern recognition, pp. 2921-2929.